Neuro-mimetic Task-free Unsupervised Online Learning with Continual Self-Organizing Maps

Anonymous authors
Paper under double-blind review

Abstract

An intelligent system capable of continual learning is one that can process and extract knowledge from potentially infinitely long streams of pattern vectors. The major challenge that makes crafting such a system difficult is known as *catastrophic forgetting* – an agent, such as one based on artificial neural networks (ANNs), struggles to retain previously acquired knowledge when learning from new samples. Furthermore, ensuring that knowledge is preserved for previous tasks becomes more challenging when input is not supplemented with task boundary information. Although forgetting in the context of ANNs has been studied extensively, there still exists far less work investigating it in terms of unsupervised architectures such as the venerable self-organizing map (SOM), a neural model often used in clustering and dimensionality reduction. While the internal mechanisms of SOMs could, in principle, yield sparse representations that improve memory retention, we observe that, when a fixed-size SOM processes continuous data streams, it experiences concept drift. In light of this, we propose a generalization of the SOM, the continual SOM (CSOM), which is capable of online unsupervised learning under a low memory budget. Our results, on benchmarks including MNIST, Kuzushiji-MNIST, and Fashion-MNIST, show almost a two times increase in accuracy, and CIFAR-10 demonstrates a state-of-the-art result when tested on (online) unsupervised class incremental learning setting.

1 Introduction

A major hurdle in designing autonomous, continuously learning agents is ensuring that such systems effectively preserve previously acquired knowledge when faced with new information. The difficulty that agents face in retaining information acquired over time is known as catastrophic forgetting (or interference) McCloskey & Cohen (1989); Ratcliff (1990); McCloskey & Cohen (1989) and is a significant challenge in the problem setting known as lifelong or continual learning Thrun & Mitchell (1995); Chen & Liu (2016); Masana et al. (2023); Ororbia et al. (2020; 2022). In continual learning, an agent must embed knowledge learned from data in a sequential manner without compromising prior knowledge. Much as humans do, this agent should process samples from these sources online, consolidating and transferring the knowledge acquired over time without forgetting previously learned tasks.

Notably, catastrophic interference has been investigated with respect to deep neural networks (DNNs), which are often trained to solve supervised prediction tasks, especially in efforts such as Kirkpatrick et al. (2017); Lopez-Paz & Ranzato (2017b); Shin et al. (2017); Ororbia et al. (2020; 2022). However, a relative dearth of work exists concerning less mainstream neural systems, particularly those that conduct unsupervised learning such as self-organizing maps (SOMs) Kohonen (1982). In this work, we seek to rectify this gap by, first, studying the degree to which forgetting occurs in a classical model such as the SOM and, second, developing a generalization of this system, which we call the Continual SOM or Continual Kohonen map (*CSOM*), which is robust to the interference encountered in the context of online continual learning.

In essence, SOMs are a type of brain-inspired (or neuro-mimetic) unsupervised neural system where its neuronal units compete for the right to activate in the presence of particular input patterns, and the synaptic parameters associated with the winning unit(s) are adjusted via a form of Hebbian learning Hebb et al.

(1949); Martinetz (1993); Ororbia (2023). Notably, the SOM's units are often arranged in either a spatial format, e.g., in a Cartesian plane/grid, or in a topological fashion, e.g., in a neighborhood/field based on the Euclidean distance between the activation values of units themselves. A useful property of the SOM is that its topologically-arranged neuronal units effectively learn to construct a low-dimensional "semantic" map of the more complicated sensory input space, where similar data patterns are grouped more closely together (around particular "prototypes") and farther apart from more dissimilar ones. This makes SOMs quite useful for clustering and dimensionality reduction tasks Vesanto & Alhoniemi (2000); Bação et al. (2005); Bigdeli et al. (2022).

At first glance, it would appear that a competitive learning model such as the SOM might offer a natural immunity to forgetting since any particular neuronal unit tends to activate more often than others (by virtue of the distance function) in response to similar sensory input patterns throughout the learning process. This specialization would, in principle, result in non-overlapping, sparse representations, which have been argued to be a key way for reducing neural cross-talk Srivastava et al. (2013); Ororbia (2021), a source of forgetting McCloskey & Cohen (1989); Ratcliff (1990); French (1999). Furthermore, some approaches, such as Gepperth et al. (2015), have advocated for using SOMs in the continual learning setting. Nevertheless, as uncovered in the experiments of this paper, the SOM, in its purest form, appears to be prone to forgetting, thus motivating our particular model generalization and computational framework Mermillod et al. (2013).

In service of the problem of online continual learning, the core contributions of this paper can be summarized as:

- We adapt the classical SOM model, which was initially formulated for fitting to single static datasets, to the online continual learning setting; specifically, we study its memory retention in tandem with its ability to adapt to pattern streams. Our experiments show that the SOM experiences substantial interference across all benchmarks examined.

- We develop a generalization of the SOM, termed the CSOM, which experiences significantly less forgetting by introducing mechanisms such as specialized decay functionality and running variance to select the best matching unit (BMU) for an input at a given time step.

- We present experimental results for four class-incremental datasets, i.e., MNIST, Fashion MNIST, Kuzushiji-MNIST, and CIFAR-10, and empirically demonstrate the robustness of the proposed CSOM to forgetting, yielding a promising, unsupervised neuromimetic system for the lifelong learning setting.

2 Related Work

In this section, we review prior work related to the central topics that drive this paper: general principles of competitive learning, self-organizing maps, and continual unsupervised learning.

Competitive Learning. In competitive learning Hartono (2012), neurons compete with each other to best match with encountered input sample patterns. This form of neural computation is often built on top of Hebbian learning Hebb et al. (1949); Choe (2013); Ororbia (2023) (where an adjustment made to a synapse depends on only local information that is available to it both spatially and temporally) and is typically used to perform clustering on input data. Vector quantization Gray (1984) and self-organizing maps (Kohonen maps) Kohonen (1982) are prominent examples within this family of models. Unlike modern-day DNNs, where all internal neurons participate in every step of inference and learning, in competitive learning, only the neurons that satisfy certain criteria "win" the right to compute Srivastava et al. (2013) and update their connection weight strengths. This form of learning can be useful in identifying and extracting useful features within a dataset. According to Rumelhart et al. (1986); Ororbia (2023), three fundamental elements define competitive learning in general: **1**) the model starts with a set of units that are highly similar, except for some random noise, which makes each of them respond slightly differently to a set of inputs; **2**) there is a limit to the "strength" of each unit (which motivates the notion of neighborhood functions, as discussed later); and **3**) the units are allowed to compete in some way for the right to respond to a particular subset of inputs.

Self-Organizing Maps. The self-organizing map (SOM) Kohonen (1982), and its many variants Khacef et al. (2020); Rougier & Detorakis (2021); Kopczyński (2021); Gliozzi & Plunkett (2018), is an unsupervised clustering neural model that adjusts its connection strengths via a Hebbian update rule Hebb et al. (1949). During training, spatially arranged clusters gradually form around the best-matching neurons within the SOM. This allows the SOM to be useful as a data exploration tool and even as an effective minimally supervised learner Lyu et al. (2024), wherein its internal units represent a summary of the latent patterns found within a dataset. In contrast to clustering algorithms, such as K-means Forgy (1965); Lloyd (1982), SOMs perform a soft clustering over inputs, which means that the connection weight update for the best matching neuron is the strongest while the updates made to the others decay/fade gradually as one moves farther away to other neurons within the best matching neuron's neighborhood.

SOMs, in the view of this study, make potentially invaluable memory systems of sensory input patterns given that they iteratively compress their information into compact parameter vectors (or neural "templates") as opposed to the raw data buffers Boschini et al. (2023); Wang et al. (2023) generally used for storing clusters or exemplars of specific task datasets, much like those often used in many continual learning methods Hayes et al. (2019); Lopez-Paz & Ranzato (2017b). Furthermore, as has been shown in prior work Bashivan et al. (2019); Pinitas et al. (2021b), the SOM's learning process is better equipped to facilitate the capture of the subtle differences (or variance) across a task's constituent data patterns.

Continual Unsupervised Learning. One of the applications of continual learning is to design agents capable of performing intelligent operations on low-resource or edge-computing devices, such as those generally found in self-driving cars Liu et al. (2019) or robotic control systems. Like many other real-world sources, self-driving cars generate enormous quantities of data that are often unlabeled or unannotated. Therefore, the value of unsupervised learning is relatively high for these kinds of applications. A consequence is that effort will be required to obtain optimized solutions to tackle the problem of catastrophic forgetting in unsupervised learning.

Crafting probabilistic generative models Shin et al. (2017); Ye & Bors (2023) that are capable of synthesizing data samples, which can be used to refresh the memory of task-specialized neural models (e.g., a classifier/regressor), is one prevalent approach. Ayub & Wagner (2021) employed (neural) encoder models to store the centroids of task data, which were later used to generate data from previous tasks in order to induce replay. However, this approach is not computationally feasible for large quantities of data – storing multiple encoder models per task results in an increase in memory complexity as well as incurs additional computational time needed to train each additional new encoder network for every newly encountered task. This greatly hinders the scalability of such an approach. In general, rehearsal-based approaches Rebuffi et al. (2017); Isele & Cosgun (2018), of which some schemes could technically be considered to fall under the umbrella of unsupervised continual learning, often store data samples in some form of explicit memory. However, low-resource devices often do not have a large memory capacity to store (enough) samples that adequately capture the variance of every task's distribution; therefore, this reduces such schemes' effectiveness given that explicitly storing more data to facilitate effective (memory-based) refreshing/retraining of more complex neural predictor model is not feasible Li et al. (2023).

In this work, we will show that our proposed CSOM can readily and usefully capture the variance inherent to each task's dataset (within a sequence) and yet not need constant, expensive retraining or refreshing itself. Finally, although out of scope for this paper, we remark that the SOM models we study could also be made to expand much as in (growing, Xu et al. (2022); Ye & Bors (2023); Yang et al. (2023)) dynamical neural gas models Fritzke (1994); Ventocilla et al. (2021)

3 Methodology

Notation. We start by defining the notation that will be used throughout this paper. $\odot$ indicates a Hadamard product, $\cdot$ indicates a matrix/vector multiplication (or dot product if the two objects it is applied to are vectors of the same shape). $||\mathbf{v}||_p$ is used to represent the p-norm (distance function w.r.t. the difference between two vectors), i.e., $p = 2$ selects the 2-norm or Euclidean distance. $\mathbf{W}[:, i]$ is the slice operator, meant to extract the ith column vector of matrix $\mathbf{W}$; $\mathbf{W}[i, :]$ is meant to extract the ith row. $\cos(\theta)$ indicates cosine similarity.

Algorithm 1 The inference and learning processes for the (classical) SOM, formulated for the online stream setting.

Input: sample $\mathbf{x}_i^{(k)}(t)$, synaptic weights $\mathbf{M}$, topology $\mathcal{G}$, simulation time step t
Parameter: $\lambda, \sigma, \tau_\lambda, \tau_\sigma, \lambda_{t=0} \leftarrow \lambda, \sigma_0 \leftarrow \sigma$

function UPDATE($\mathbf{x}_i^{(k)}(t)$, $\mathbf{M}$, $\mathcal{G}$, σ_t, λ_t) ▷ Compute L2 distances and perform weighted updates
  $\mathbf{\Delta_2} = \mathbf{x}_i^{(k)}(t) - \mathbf{M}$, $\mathbf{d} = ||\mathbf{\Delta_2}[:, j]||_2, j = 0, 1, ...H$ ▷ Compute the BMU, u and its neighbors, $\mathcal{N}_u$
  $u = \arg\min_{j \in H} \mathbf{d}$, $\mathcal{N}_u = \text{GETNEIGH}(u, \mathbf{M}, \mathcal{G})$
  for $v_j \in (u \cup \mathcal{N}_u)$ **do** ▷ Update synapses of the BMU and its neighbors
    $\mathbf{M}[:, v_j] \leftarrow \mathbf{M}[:, v_j] + \lambda_t \phi(u, v_j, \mathcal{G}, \sigma_t)(\mathbf{\Delta}[:, v_j])$
function TRAIN($\mathbf{x}_i^{(k)}(t), \mathbf{M}, \mathcal{G}, t$) ▷ Online training routine TRAIN(.), at time step t
  $\lambda_t = \lambda_0 \exp(-t/\tau_\lambda)$ ▷ or use Equation 1
  $\sigma_t = \sigma_0 \exp(-t/\tau_\sigma)$ ▷ or use Equation 2
  UPDATE($\mathbf{x}_i^{(k)}(t), \mathbf{M}, \mathcal{G}, \sigma_t, \lambda_t$) ▷ inference step
  $t \leftarrow t + 1$ ▷ Advance simulation time forward

Problem Definition. Consider a sequence of T tasks, which we formally denote by $\mathcal{S} = \bigcup_{k=1}^{T} \mathcal{T}_k$. Each task $\mathcal{T}_k$ has a training dataset (each containing C classes), $\mathcal{D}_{train}^{(k)} = \bigcup_{i=1}^{N_k} \{(\mathbf{x}_i^{(k)}, \mathbf{y}_i^{(k)})\}$, where $\mathbf{x}_i^{(k)} \in \mathcal{R}^{D \times 1}$ is a data pattern and $\mathbf{y}_i^{(k)} \in \{0, 1\}^{C \times 1}$ is its label vector. Furthermore, we let N_k be the number of patterns in task T_k and $\mathcal{D}_{test}^{(k)}$ to represent the test dataset for task $\mathcal{T}_k$. We remark that, although the datasets investigated in this work come with labels, our models will never use them since they are unsupervised. However, we will use the labels for external analysis, as we will see in our defined metric(s). Finally, all models process each data point in $\mathcal{D}_{train}^{(k)}$ **only once (online adaptation)** and time steps are tracked in simulation within the variable t, i.e., each time that a data point $\mathbf{x}_i^{(k)}$ is sampled from $\mathcal{D}_{train}^{(k)}$ of task $\mathcal{T}_k$, t is incremented as $t \leftarrow t + 1$.

When a continual learning agent is finished training on task $\mathcal{T}_k$ (using $\mathcal{D}_{train}^{(k)}$), the data $\mathcal{D}_{train}^{(k)}$ will be lost as soon as the model proceeds to task $\mathcal{T}_{k+1}$ (up to $\mathcal{T}_T$). Furthermore, note that $\mathcal{D}_{test}^{(k)}$ is only used for external model evaluation. The general objective/goal is to maximize the agent's generalization performance on task $\mathcal{T}_k$ while minimizing how much its performance degrades on prior tasks $\mathcal{T}_1$ to $\mathcal{T}_{k-1}$.

3.1 The Kohonen Map

In Algorithm 1, we present our formulation of the classical SOM (Kohonen Map) for the online processing of data points from a (task) stream. Each data point $\mathbf{x}_i^{(k)}$ is sampled from the task $\mathcal{T}_k$ (with dataset $\mathcal{D}_{train}^{(k)}$). The SOM, with H neuronal units, adapts its synaptic matrix $\mathbf{M} \in \mathcal{R}^{D \times H}$ given input $\mathbf{x}_i^{(k)}$. In this study, the topology $\mathcal{G}$ is a square grid of dimensions $K \times L$ (i.e., $H = K * L, K = L$). $\phi(u, v_j, \mathcal{G}, \sigma_t)$ indicates a neighborhood weighting function used to scale the update to unit v_j with synaptic vector $\mathbf{M}[:, v_j]$. Note that the weighting function depends on the euclidean distance between the BMU (u) and the neighboring units (v_j) in the cartesian plane.

Specifically, we see that inference is conducted in the UPDATE() routine of Algorithm 1. The SOM first computes the (Euclidean) distance between the current sample $\mathbf{x}_i^{(t)}$ and all internal units in $\mathbf{M}$ and then stores these distances in the distance (row) vector $\mathbf{d} \in \mathcal{R}^{1 \times H}$. The BMU is calculated by taking the argmin over $\mathbf{d}$, returning the index of the BMU as integer u[1] Finally, the indices/coordinates of the neighboring units of BMU – any such neighbor is indexed by v_j – are returned by the GETNEIGH() sub-routine and stored in the array $\mathcal{N}_u$.

To update the relevant synaptic weight vectors of the SOM's matrix $\mathbf{M}$, a loop runs through unit indices ($u \bigcup \mathcal{N}_u$) and a weighted Hebbian update is applied. Note that the Hebbian rule in Algorithm 1 reuses the

[1]Note that u further maps to a fixed two-dimensional coordinate (k_u, l_u), where $0 < k_u \leq K$ and $0 < l_u \leq L$, since $\mathcal{G}$ is rectangular in our formulation of SOMs.

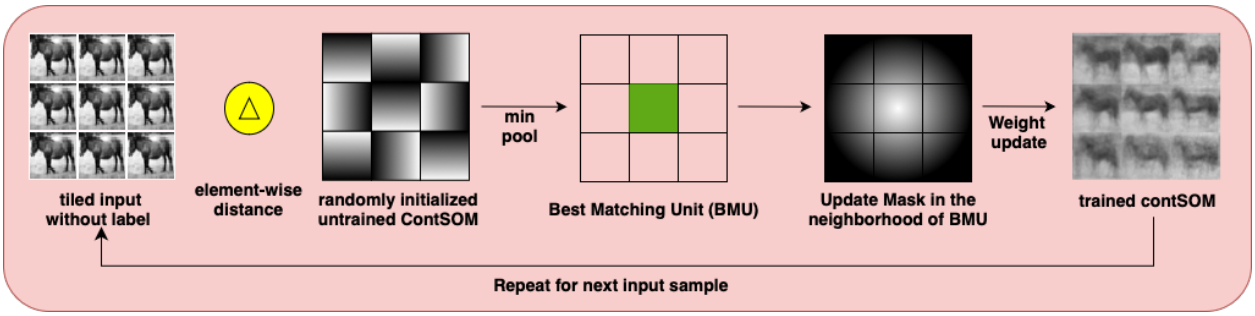

Figure 1: Illustration of the overall process for best-matching unit (BMU) selection and synaptic updating of the CSOM for unsupervised online learning.

difference vectors stored in $\mathbf{\Delta}$ and applies both a dynamic learning rate λ_t and a coefficient produced by $\phi(u, v_j, \mathcal{G}, \sigma_t)$. The neighborhood function $\phi(u, v_j, \mathcal{G}, \sigma_t)$ was set to be a Gaussian function, centered around the BMU indexed by u, with radius σ_t. Note that the **classical SOM maintains one global copy of learning rate λ_t and radius σ_t that is shared among all neurons**. They are designed to be dynamic, time-dependent functions and are shown in the Train() routine (which also depicts the full training step performed by our online SOM). We found, through empirical study, that the following set of equations yielded better clusters as opposed to original decay functions of Kohonen (1982):

$$\lambda_t = \lambda_0(1 + t * \exp(t/\tau_\lambda))^{-1} \tag{1}$$

$$\sigma_t = \sigma_0(1 + t * \exp(t/\tau_\sigma))^{-1}. \tag{2}$$

3.2 The Continual Kohonen Map

In Algorithm 2, we present our proposed model, the continual SOM (CSOM [2], Figure 1), built to process and generalize dynamically from samples drawn from a stream of tasks. Notice that, first of all, the CSOM now maintains an additional (non-negative) matrix $\mathbf{M}^{\omega^2} \in \mathcal{R}_+^{D \times H}$, which contains synaptic weight parameters associated with the "running variance" (ω^2) of each neuronal unit in the system. This means that each unit/prototype in the CSOM is defined by two vectors of weights – one for approximate unit means and another for approximate standard deviations. The intuition is that each unit in our SOM model is generalized to maintain its own learnable multivariate Gaussian distribution (inspired by the latent variables of incremental Gaussian mixture models) with a diagonal covariance matrix. Notice that, in the Update() routine of our CSOM, the variance parameters are adjusted using a Hebbian-like rule inspired by Welford's online algorithm Welford (1962) but modified to use the weighting provided by our CSOM's neighborhood function. We denote the initial scaling/update factor for running variance of every unit as λ_ω^0 as shown in step 11 of Algorithm 2. In SOMs, the ratio of weight update that each connection goes through depends on its distance from the BMU. In CSOM, we empirically found that the update/scaling factor of running variance of every neuron is proportional to the magnitude of its weight update. Therefore, this update factor for a neuron is decayed as per its distance from the BMU to obtain λ_ω in step 11 of Algorithm 2. The running variance vector coupled to every neuron in the CSOM can be used to generate samples belonging to the class that matched it. Thus, the underlying structure of our neural system could be likened to a simple, dynamic generative model.

In addition to the local running variance parameters, the CSOM is designed to promote a form of neuronal competition driven by unit-centric learning and distance weighting parameters. **Specifically, each neuron $h \in H$ arranged in topology $\mathcal{G}$ is assigned an independently-controlled, dynamic radius σ_h and learning rate λ_h parameter (as shown in Figure 2)**. As shown in Algorithm 2, in the routine Update(), we particularly decay learning parameters only for the BMU (u), i.e., only σ_u and λ_u are decayed at time t. This localized decay is furthermore a function of the number of times that unit u has been selected as the BMU, i.e., unit u adjusts σ_u and λ_u as a function of its BMU count η_u. We do not decay σ_u and λ_u

[2]All the notations are summarized in Table 5

Algorithm 2 CSOM inference and learning processes.

Require: data sample $\mathbf{x}_i^{(k)}(t)$, SOM weight matrix $\mathbf{M}$, running variance matrix $\mathbf{M}^{\omega^2} \in \mathcal{R}^{D\times H}$, radius σ_v, σ_V, learning rate λ_h, BMU count for a unit (η_u is count for unit u)

Note: HTile$(\mathbf{x}, H)$ tiles vector $\mathbf{v}$ H times horizontally; VTile$(\mathbf{x}, H)$ tiles vector $\mathbf{x}$ H times vertically, $d(a, b; \mathcal{G})$ is a distance over topology $\mathcal{G}$, where a maps to (a_i, a_j) (2D coordinate) and b maps to (b_i, b_j)

function UPDATE$(\mathbf{X}_i, u, V, \sigma_u^{(t)}, \lambda_u^{(t)}, \mathbf{M}, \mathbf{M}^{\omega^2}, \mathcal{G})$

$\delta = (2 * \sigma_u^2)^{-1}$

$\tau_1 = -\delta^{-1} * \log\left(\frac{10^{-8}}{\lambda_u}\right)$

$\mathbf{o}_{1,v_j} = \begin{cases} 1 & d(v_j, u; \mathcal{G}) < \sigma_u \\ 0 & \text{otherwise} \end{cases}$ ▷ v_j is any non-BMU neuron, $\mathbf{o} \in \{0,1\}^{1\times H}$ (masking vector)

$\mathbf{s}_{1,j} = \begin{cases} \lambda_u & j = u \\ \lambda_v & j = v_j \end{cases}$ ▷ $\mathbf{s} \in \mathcal{R}^{1\times H}$ learning rate vector

$\phi = \text{VTile}\Big(\{\mathbf{o}_{v_j}\mathbf{s}_{v_j} \exp\left[-d(u, j; \mathcal{G})\delta\right], \text{ for } j = 1, 2, ..., H\}, D\Big)$ ▷ $\phi \in \mathcal{R}^{D\times H}$

$\mathbf{M} = \mathbf{M} + \phi \odot (\mathbf{X}_i - \mathbf{M})$ ▷ CSOM update step

$\eta_u = \eta_u + 1$

$\lambda_\omega = \text{VTile}\Big(\{(\lambda_\omega^0 - 0.5) + (1 + \exp\left(-d(u, j; \mathcal{G})/\tau_1\right))^{-1}, \text{ for } j = 1, 2, ..., H\}, D\Big)$ ▷ $\lambda_\omega \in \mathcal{R}^{D\times H}$

$\lambda_\omega = \lambda_\omega \odot \mathbf{O} + (1 - \mathbf{O})$, where $\mathbf{O} = \text{VTile}(\mathbf{o}, D)$ ▷ scaling factor for updating running variance

$\mathbf{M}^{\omega^2} = \lambda_\omega \mathbf{M}^{\omega^2} + (1 - \lambda_\omega)(\mathbf{X}_i - \mathbf{M})^2$ ▷ update running variance of all neurons

$\sigma_u^{(t)} = \sigma_u^{(t-1)} \exp\left(\eta_u/\tau_\sigma\right)$ ▷ $\tau_\sigma \leftarrow$ constant

$\lambda_u^{(t)} = \lambda_u^{(t-1)} \exp\left(\eta_u/\tau_\lambda\right)$ ▷ $\tau_\lambda \leftarrow$ constant

function TRAIN$(\mathbf{x}_i^{(k)}(t), \mathbf{M}, \mathbf{M}^{\omega^2}, \mathcal{G}, t)$

$\mathbf{X}_i \leftarrow \text{HTile}(\mathbf{x}_i^{(k)}(t), H)$ ▷ tile/repeat $\mathbf{x}_i^{(t)}$ H times horizontally to create $\mathbf{x}_i^{(k)}(t) = \mathbf{X}_i \in \mathcal{R}^{D\times H}$

$\mathbf{\Delta}_\omega = (\mathbf{X}_i - \mathbf{M})^2/\mathbf{M}^\omega$ ▷ distance calculation specific to CSOM , $\mathbf{M}^\omega = \sqrt{\mathbf{M}^{\omega^2}}$

$\mathbf{d} = \Delta_\omega[i, j]$ ▷ $i \in \{1, 2, ..K\}$ and $j \in \{1, 2, ..L\}$

$u = \arg\min_{h\in H} \mathbf{d}$ ▷ BMU calculation

UPDATE$(X_i, u, V, \sigma_u^{(t)}, \lambda_u^{(t)}, \mathbf{M}, \mathbf{M}^{\omega^2}, \mathcal{G})$ ▷ $V = H \setminus u$ (i.e., V is set of all non-BMU indices)

after they reach certain infinitesimally small threshold to ensure their values do not plummet to 0 and some positive weight update is always achieved as $t \to T$. The neighborhood function of the CSOM is also notably a function of the running variance parameters $\mathbf{M}^{\omega^2}$, further facilitating the calculation of a per-unit region of influence (treating each neuron as its own weighted multivariate Gaussian distribution). As a result, whenever a weight update is triggered, synaptic values are adjusted on a linear scale for the BMU u while, for any non-BMU units v_j, the update is adjusted on a scale that decreases as the euclidean distance from u increases. The CSOM utilizes a masking matrix ($\mathbf{o}$) to control the scale of its synaptic weight updates. The mask matrix also prevents any leaky weight updates caused by infinitesimally small values passed by the neighborhood function (ϕ).

Crucially, the proposed CSOM is a task-free model Masana et al. (2023); Aljundi et al. (2018), which means that it does not require any information about task boundaries (in the form of task descriptors). In addition, the CSOM, much like our reformulation of the SOM described earlier, is constructed to process data in an online, iterative fashion, adapting its per-unit parameters as a function of simulation time.

4 Mathematical Analysis

In this section, we formally show that the CSOM reaches an equilibrium state or fixed point Haag et al. (1974); Stogin et al. (2024); Burton (2003), meaning that it exhibits stability, a quality that improves its generalization ability as well as helps it avoid catastrophic forgetting.

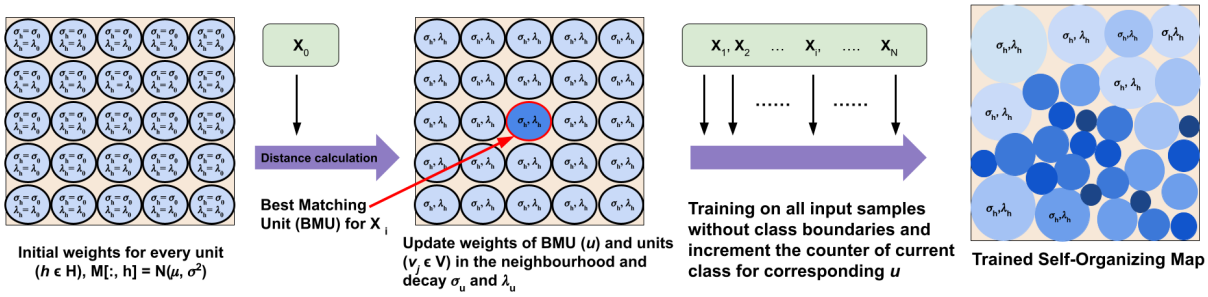

Figure 2: Unit centric parameter update in CSOM inspired from competitive learning

Given the variance update rule in the continual self-organizing map (CSOM) described in the previous section, reproduce below as follows (for an arbitrary pattern vector sampled at time t):

$$\omega_i^2(t+1) = \lambda_\omega \cdot \omega_i^2(t) + (1-\lambda_\omega) \cdot (\mathbf{x}(t) - \mathbf{M}_i(t))^2,$$

where $\lambda_\omega \in (0,1)$ is the learning rate, we analyze the convergence of the series defining $\omega_i^2(t)$.

Lemma: Convergence of the Variance Series

Lemma 4.1 *The series for $\omega_i^2(t)$ converges under the assumption that the sequence of squared deviations $(\mathbf{x}(t) - \mathbf{M}_i(t))^2$ is bounded.*

Proof: Expanding the recurrence relation yields the following:

$$\omega_i^2(t+1) = \lambda_\omega^t \cdot \omega_i^2(1) + (1-\lambda_\omega) \sum_{k=0}^{t} \lambda_\omega^k \cdot \big(\mathbf{x}(t-k) - \mathbf{M}_i(t-k)\big)^2.$$

Assuming the sequence $\big(\mathbf{x}(t) - \mathbf{M}_i(t)\big)^2$ is bounded by some value $M > 0$, we analyze the convergence of the resultant geometric series:

$$\sum_{k=0}^{\infty} \lambda_\omega^k \cdot (\mathbf{x}(t-k) - \mathbf{M}_i(t-k))^2.$$

Given $0 < \lambda_\omega < 1$, the following series:

$$\sum_{k=0}^{\infty} \lambda_\omega^k$$

is a convergent geometric series. By the comparison test, our series converges since each term is bounded by $\lambda_\omega^k \cdot M$.

Hence, the series defining $\omega_i^2(t)$ converges, particularly indicating that $\omega_i^2(t)$ stabilizes as $t \to \infty$, contributing to the SOM's capability to mitigate catastrophic forgetting by maintaining an adaptive and stable measure of variance. □

Next, we move to showing the convergence of the synaptic weight vectors of the proposed CSOM.

Proposition 4.2 *For the weight vectors $\mathbf{M}_i(t)$ in a continual self-organizing map (CSOM) updated by the rule:*

$$\mathbf{M}_i(t+1) = \mathbf{M}_i(t) + \lambda_i \cdot \phi(t,u,i) \cdot (\mathbf{x}(t) - \mathbf{M}_i(t)),$$

where $\lambda_i \in (0,1)$ is a fixed learning rate, u is the (integer) index of the best matching unit, and $\phi(t,u,i)$ is a neighborhood function[3]*, it holds that*

$$\|\mathbf{M}_i(t+1) - \mathbf{M}_i(t)\| \to 0$$

[3]Note that, in Algorithm 2, we set this to be $\phi(t,u,i) = d(u,i)$.

as $t \to \infty$, indicating the convergence of the model's synaptic weight vectors.

Proof: The difference between successive weight vectors is given by:

$$\Delta \mathbf{M}_i(t) = \mathbf{M}_i(t+1) - \mathbf{M}_i(t) = \lambda_i \cdot \phi(t, u, i) \cdot \big(\mathbf{x}(t) - \mathbf{M}_i(t)\big).$$

To demonstrate convergence, we need to show that $\|\Delta \mathbf{M}_i(t)\| \to 0$ as $t \to \infty$.

1. **Bounding the Update Magnitude:** Notice that $\|\Delta \mathbf{M}_i(t)\|$ is bounded above by $\lambda_i \cdot \|\phi(t, i) \cdot (\mathbf{x}(t) - \mathbf{M}_i(t))\|$. Since $\lambda_i \in (0, 1)$ and assuming $\phi(t, u, i)$ is designed to decrease over time and as the distance from the BMU increases, then $\|\phi(t, u, i) \cdot (\mathbf{x}(t) - \mathbf{M}_i(t))\|$ also decreases.

2. **Decrease Over Time:** As t increases, the influence of $\phi(t, u, i)$ diminishes, which in turn reduces the magnitude of $\Delta \mathbf{M}_i(t)$. This reduction is due to the adaptation of the weight vectors to the distribution of the input pattern vectors, leading to smaller corrections required over time as the neural map stabilizes.

3. **Limiting Behavior:** Given that the sequence of input vectors $\{\mathbf{x}(t)\}$ is bounded (a common assumption in many applications of the SOM), and the learning rate λ_i is fixed or changes at steady rate ($\lambda_i > 0$), the product $\lambda_i \cdot \phi(t, u, i)$ ensures that the updates to $\mathbf{M}_i(t)$ decrease in magnitude. Hence, $\|\Delta \mathbf{M}_i(t)\| \to 0$ as $t \to \infty$.

Therefore, the synaptic weight vectors $\mathbf{M}_i(t)$ converge as evidenced by the decrease in the magnitude of the updates between successive time steps, confirming the proposition. □

Next, we show that the CSOM reaches an equilibrium state as well as reaches a fixed point, indicating its continual adaptation of knowledge:

Theorem 4.3 *Equilibrium in a continual self-organizing map (CSOM) is achieved through the calibration of the learning rate values λ_ω and λ_i, alongside the topological considerations enforced by the neighborhood radius σ_u as well as the neighborhood function $\phi(t, u, i, \sigma_u)$. This calibrated mechanism facilitates the CSOM's adaptation to new input patterns while allowing it retain critical information about the distribution of past inputs, thus mitigating catastrophic forgetting.*

Proof: The proof of the above theorem focuses on the stabilization brought about by these parameters:

1. Learning Rate Impact: The learning rates λ_ω and λ_i directly influence the rate of adaptation for variance and weight vectors, respectively. A careful balance of these rates ensures that the CSOM network remains sensitive to new inputs without rapidly discarding historical data.

2. Neighborhood Radius and Function: The neighborhood radius σ_u, which typically decreases over time, determines the extent to which the neighborhood surrounding the BMU is affected by each input pattern. The neighborhood function $\phi(t, u, i, \sigma_u)$ modulates the update magnitude based on σ_u and the neuron's distance from the BMU, ensuring a cohesive topological adaptation across the network.

Mathematical Justification: The equilibrium condition, characterized by diminishing updates to both variance and weight vectors, is achieved when $\|\omega_i^2(t+1) - \omega_i^2(t)\| \to 0$ and $\|\mathbf{M}_i(t+1) - \mathbf{M}_i(t)\| \to 0$ as $t \to \infty$. The decrease in σ_u over time reduces the influence of new inputs on distant neurons, contributing to the network's overall stability.

Conclusion: Through the interplay of λ_ω, λ_i, σ_u, and $\phi(t, u, i, \sigma_u)$, the SOM achieves a dynamic equilibrium. This balance between sensitivity to new data and the retention of historical patterns allows the CSOM to adaptively map its input space (to neuronal unit space) while mitigating the risk of catastrophic forgetting.

□

Finally, we formally show that the CSOM and its proposed synaptic update rule help the model to mitigate forgetting and learn new features without compromising prior knowledge:

Theorem 4.4 *Given a sequence of input vectors $\{\mathbf{x}(t)\}_{t=1}^{\infty}$ where $\mathbf{x}(t) \in \mathbb{R}^D$, and a continual self-organizing map (CSOM) with H neurons, each neuron i characterized by a weight vector $\mathbf{M}_i \in \mathbb{R}^D$ and a running variance $\omega_i^2 \in \mathbb{R}$, updated at each time t by:*

1. Variance Update Rule:

$$\omega_i^2(t+1) = \lambda_\omega \cdot \omega_i^2(t) + (1 - \lambda_\omega) \cdot (\mathbf{x}(t) - \mathbf{M}_i(t))^2,$$

2. Synaptic Weight Update Rule:

$$\mathbf{M}_i(t+1) = \mathbf{M}_i(t) + \lambda_i \cdot \phi(t, u, i) \cdot (\mathbf{x}(t) - \mathbf{M}_i(t)),$$

with $\lambda_\omega, \lambda_i \in (0, 1)$ as learning rates, and $\phi(t, u, i)$ as the neighborhood function, then the SOM achieves a dynamic equilibrium, enhancing its stability and mitigating catastrophic forgetting.

Proof: The proof consists of three key parts:

Part 1: Variance Stability. The exponential decay factor $(1 - \lambda_\omega)$ ensures that older inputs have a diminishing influence on the running variance $\omega_i^2(t)$. For large t, this stabilizes, indicating the SOM's ability to incorporate new variance information without losing the significance of past data variance. Mathematically, this can be shown by analyzing the series convergence of $\omega_i^2(t)$, which was demonstrated in Lemma 4

Part 2: Convergence of Synaptic Weight Vectors. The weight vectors $\mathbf{M}_i(t)$ are updated towards (the direction of) new inputs with a learning rate that is modulated by $\phi(t, i)$, ensuring that neurons closer to the BMU have a higher rate of adaptation. This promotes the stability and convergence of $\mathbf{M}_i(t)$, which is crucial for maintaining knowledge of learned patterns over time. The convergence can be argued by demonstrating that the updates lead to a decrease in the difference between successive weight vectors, $\|\mathbf{M}_i(t+1) - \mathbf{M}_i(t)\| \to 0$ as $t \to \infty$, as was formally proven in Proposition 4.

Part 3: Dynamic Equilibrium and the Mitigation of Catastrophic Forgetting. Combining the effects of the variance and synaptic weight updates, the CSOM maintains a balance between adapting to new (sensory) data and preserving information about the distribution of the past inputs it has encountered. This equilibrium is achieved through the careful calibration of λ_ω and λ_i, alongside the topological considerations enforced by $\phi(t, u, i)$, as shown in Theorem 4.

Thus, this mathematical framework ensures that the CSOM's neuronal units' updates are such that neither new nor old information is disproportionately favored, which mitigates catastrophic forgetting. Therefore, by the specified update rules and their mathematical properties, the CSOM achieves a dynamic equilibrium that effectively mitigates catastrophic forgetting. □

5 Experiments

To test our proposed CSOM and determine its performance on competitive datasets, we performed experiments across three databases under two continual learning setups.

5.1 Datasets

To evaluate the CSOM, we employed three grayscale datasets along with one containing natural image samples.

Split MNIST, Fashion MNIST, and KMNIST: We used variations of MNIST to test our neural models – specifically, the original MNIST database LeCun et al. (1998), Fashion MNIST (FMNIST) Xiao et al. (2017), and Kuzushiji-MNIST (KMNIST) Clanuwat et al. (2018), all containing 28×28 gray-scale pixel images. Furthermore, we transformed these datasets by normalizing them, i.e., diving them by 255.0, which brought them into the value range of $[0.0, 1.0]$, thus making the learning process easier for the SOMs/CSOM models.

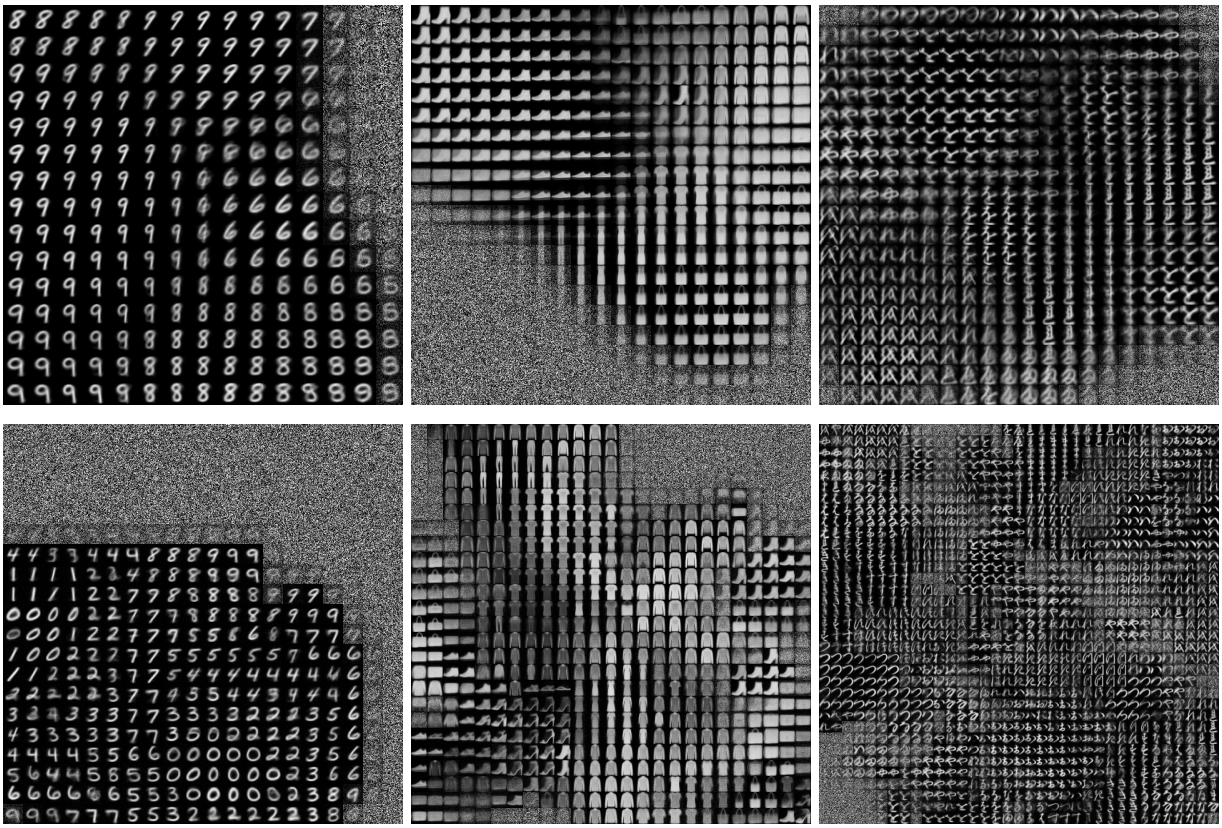

Figure 3: Class-incrementally adapted classical SOM (top row) versus continual SOM (bottom row) on: MNIST (Left), FashionMNIST (Middle), and KMNIST (Right).

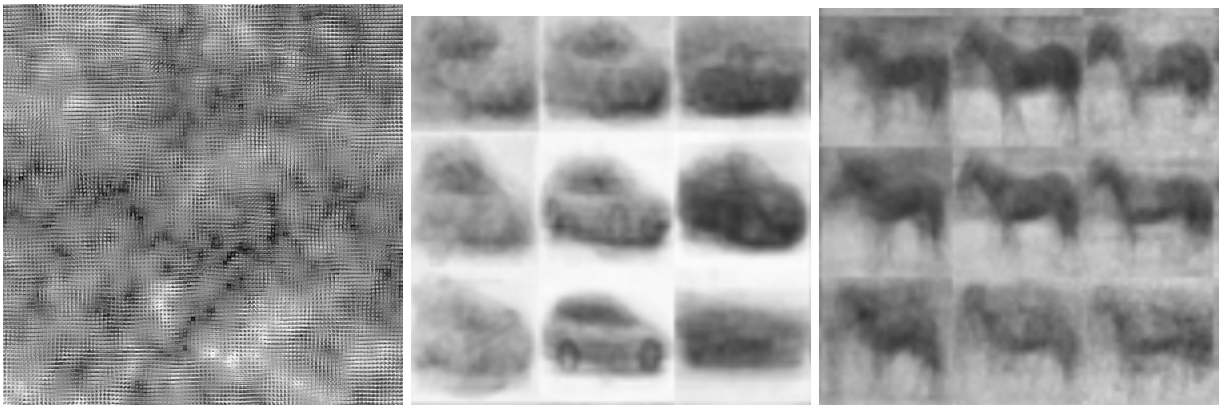

Figure 4: (Left) CSOM containing 100x100 neurons/units trained class incrementally on grayscale images of CIFAR-10. (Right) Two snapshots of trained CSOM clusters

Split CIFAR-10: To test the CSOM on images belonging to different (more complex) distributions, we also utilized the CIFAR-10 dataset Krizhevsky & Hinton (2010), which contains a large number of samples with 32×32 Red-Green-Blue (RGB) images. We specifically converted the CIFAR-10 images to grayscale to test the neural models of this study (and defer the use of separate color channels for future work). Furthermore, we normalized the images as in the MNIST datasets, bringing their pixel values into the range of $[0.0, 1.0]$.

Model	$(K = L)$	σ_0	λ_0	ω_0^2	λ_ω^0
Vanilla SOM	[15, 20, 20]	0.6	0.07	1	0
DendSOM	[10, 10, 10]	1.5	0.07	0	0
CSOM	[15/20, 25, 35]	1.5	0.07	0.5	0.9

Table 1: Parameter setting for the architectures and their training

Model Baselines: We adapt the Dendritic SOM (DendSOM) Pinitas et al. (2021a), further utilizing their label prediction method to evaluate the performance of our proposed model. The DendSOM uses a hit matrix to determine the label of a trained unit in the evaluation phase. We maintain a similar hit matrix (BMU count, η_u) later used in the evaluation phase for label prediction. This ultimately helps us to establish a fair comparison between our model and baselines.

5.2 Learning Simulation Setups

Class Incremental Learning: In this study, we focus on the continual learning setup where tasks consist of data points belonging entirely to one single class. Specifically, this means that for any given task $\mathcal{T}_t$, its training dataset $\mathcal{D}_{train}^{(t)}$ contains all data points labeled under one specific class $c \in C$ (where C is the total number of unique classes in the entire benchmark dataset). For instance, for the case of Split-MNIST, this means that task $\mathcal{T}_0$ consists entirely of patterns with the class label of the digit zero, and task $\mathcal{T}_1$ consists entirely of the digit one, and so on and so forth. Furthermore, note that all models and baselines studied are trained under the same setup with the same seeding/shuffling of data points in order to ensure a fair comparison. All models are trained to process the data points incrementally/online, one sample at a time, and no data points are ever revisited (meaning that each model is only allowed one single epoch or pass through an entire task data subset, effectively simulating the online streaming learning setting Agarwal et al. (2008); Beyazit et al. (2019)).

Domain Incremental Learning: In this setup we simulated a domain incremental learning within a given dataset. This is similar to a task incremental setup; however, here, we divided the datasets into five tasks, where each task had data samples representing two digits, labeled in binary, i.e., $c \in [0, 1]$ (0 encoded class one, 1 encoded class two).

5.3 Training and Architecture Parameters

We followed a square design for the topology underlying all of the models examined in this work. This means that every SOM/CSOM had $K \times L$ units in its topology, $(K = L)$. In Table 1, the column for $(K = L)$ indicates values of K for MNIST, Fashion-MNIST, KMNIST, respectively. The initial value of the running variance for all pixels in every SOM unit (ω_0^2) was decided based on the distribution of pixels in the input dataset. We found empirically that setting ω_0^2 slightly higher than the variance of input distribution gave us a good starting point. Similarly, setting λ_ω^0 within the range $[0.9, 0.99]$ helped to maintain an effective balance between the old and new values of the running variance at every simulation step. For the DendSOM, we modeled/instantiated four copies of SOM (M) where the unit topology size in each copy was $[14 \times 14]$. Since the DendSOM breaks the input image into patches for every copy of SOM, the easiest way to divide an MNIST-type of image having dimensions $[28 \times 28]$ would be to have its four patches be of shape $[14 \times 14]$. We followed this for the implementations of DendSOM presented in our work. Through a brute force approach, we found that setting $\tau_\sigma = 8$ and $\tau_\lambda = 45$ performed a gradual decay of σ and λ throughout training.

5.4 Evaluation

For model evaluation, we adapted the point-wise mutual information (PMI) Pinitas et al. (2021a) measure, which loosely follows the Hebbian rule of learning to suit the design logic of CSOM. Formally, the PMI is

calculated as follows:

$$PMI(l; BMU) = \log \frac{P(l|BMU)}{P(l)} \tag{3}$$

$$P(l|BMU) = \frac{\eta[l, BMU]}{\Sigma_{i \in Labels} \eta[i, BMU]} \tag{4}$$

$$P(l) = \frac{\Sigma_{h \in Units} \eta[l, h]}{\Sigma_{h \in Units} \Sigma_{i \in Labels} \eta[i, h]} \tag{5}$$

$$Predicted\ Label = \underset{l \in Labels}{\arg\max}\, PMI(l; BMU). \tag{6}$$

The PMI of two entities could take on either a positive or negative value, depending on whether they co-occur more frequently or less frequently compared to an independence assumption. The PMI measure can become zero if the two entities are independent of each other. This PMI measure is used to predict the label of a trained unit based on a hit matrix (i.e. BMU count, η_u) which stores the number of times that a unit was selected as the BMU for any input sample. The PMI uses label information from the input samples to maintain the hit matrix that is used only at the test time for accuracy calculation; as a result, the CSOM is unsupervised in training even though its test-time performance is evaluated through a supervised lens.

Note that we measure the average accuracy of SOM models based on whether the predicted SOM/CSOM unit's label matches the input sample's expected label. Unlike the L2 distance with running variance used at training time, we employed the cosine similarity at test time in order to measure the BMU for a test input sample and to determine its predicted label. Using this method, we calculated distinct accuracy measures from test samples for each task and stored these in what is known in the continual learning literature as the accuracy task matrix (of shape $T \times T$ for T tasks). This helped us to calculate classical lifelong learning metrics such as average accuracy (ACC) Pham et al. (2024), backward transfer (BWT) Lopez-Paz & Ranzato (2017a), as well as the forgetting measure (FM) and learning accuracy (LA), both of which were mentioned in Yin et al. (2021). Formally, these evaluation metrics are defined as follows:

$$\text{ACC}(\uparrow) = \frac{1}{T} \Sigma_{i=1}^{T} a_{i,T} \qquad \text{(higher is better)} \tag{7}$$

$$\text{BWT}(\downarrow) = \frac{1}{T-1} \Sigma_{i=1}^{T-1} a_{T,i} - a_{i,i} \qquad \text{(lower is better)} \tag{8}$$

$$\text{FM}(\downarrow) = \frac{1}{T} \Sigma_{i=1}^{T} |a_{i,T} - a_i^*| \qquad \text{(lower is better)} \tag{9}$$

$$\text{LA}(\uparrow) = \frac{1}{T} \Sigma_{i=1}^{T} a_{i,i} \qquad \text{(higher is better).} \tag{10}$$

In the above equations, $a_{i,j}$ is the accuracy for task i after training on task j. The BWT measure helps us quantify how training on a new task $\mathcal{T}_k$ affects the accuracy of CSOM on the previously trained task $\mathcal{T}_{k-1}$. In other words, the BWT quantifies the amount of forgetting for a task as the training progresses incrementally for new tasks in time for any given algorithm. FM is the measure of the difference between a model's final performance and its best performance (a_i^*) for a task. LA measures the average of the current task accuracy of CSOM.

5.5 Simulation Results

In Table 2, we present our full experimental results for the three grayscale datasets. In addition, we present quantitative benchmark measurements on the CIFAR-10 dataset in Table 3, comparing to several prior, performant continual learning neural models.

The Classical SOM: As observed in Table 2, the standard/classical SOM, or "Vanilla SOM" (which indicates that no special task-driven mechanism was integrated, thus meaning that we used the online model presented in Algorithm 1), observably forgets quite strongly across all three benchmarks/datasets. In short, our results empirically confirm that, indeed, the standard SOM forgets information despite the potential (for reduced neural cross-talk) offered by its competitive internal activities. We present visual samples of the

MNIST	ACC (↑)	LA (↑)	FM (↓)	BWT (↓)
vanilla SOM	22.89 ± 0.02	46.4 ± 0.01	34.99 ± 0.01	-26 ± 0.04
DendSOM	17.13 ± 0.01	40.34 ± 0.03	23.33 ± 0.03	-25.78 ± 0.04
CSOM	**85.03 ± 4.28**	**92.26 ± 2.49**	**7.23 ± 2.42**	**-8.02 ± 2.7**
FMNIST	ACC (↑)	LA (↑)	FM (↓)	BWT (↓)
vanilla SOM	32.07 ± 0.03	57.52 ± 0.03	37.01 ± 0.03	-28.27 ± 0.02
DendSOM	16.62 ± 0.03	27.36 ± 0.03	**11.34 ± 0.03**	**-11.92 ± 0.03**
CSOM	**75.13 ± 2.68**	**88.23 ± 0.56**	13.11 ± 2.93	-14.56 ± 3.25
KMNIST	ACC (↑)	LA (↑)	FM (↓)	BWT (↓)
vanilla SOM	23.65 ± 0.03	54 ± 0.05	35.28 ± 0.01	-33.79 ± 0.02
DendSOM	10.95 ± 0.01	12.92 ± 0.01	**2.02 ± 0**	**-2.18 ± 0.01**
CSOM	**81.602 ± 2.82**	**88.61 ± 1.6**	7.04 ± 1.54	-7.78 ± 1.73

(a) Unsupervised online (epochs = 1) class incremental training

MNIST	ACC (↑)	LA (↑)	FM (↓)	BWT (↓)
vanilla SOM	55.03 ± 0.01	80.07 ± 0.02	25.59 ± 0.02	-30.71 ± 0.04
DendSOM	58.40 ± 0.03	61.37 ± 0.05	7.30 ± 0.02	**-3.7 ± 0.04**
CSOM	**89.09 ± 3.32**	**93.02 ± 2.03**	**4.03 ± 1.71**	-4.92 ± 2.11
FMNIST	ACC (↑)	LA (↑)	FM (↓)	BWT (↓)
vanilla SOM	79.36 ± 0.06	89.45 ± 0.01	12.83 ± 0.06	-12.61 ± 0.06
DendSOM	50.11 ± 0	53.13 ± 0.03	3.98 ± 0.03	-3.76 ± 0.04
CSOM	**95.61 ± 0.92**	**97.14 ± 0.4**	**1.57 ± 0.89**	**-1.92 ± 1.12**
KMNIST	ACC (↑)	LA (↑)	FM (↓)	BWT (↓)
vanilla SOM	57.18 ± 0.01	78.91 ± 0.01	21.72 ± 0.01	-27.16 ± 0.01
DendSOM	52.3 ± 0.02	54.55 ± 0.03	**3.62 ± 0.01**	**-2.8 ± 0.02**
CSOM	**88.11 ± 1.93**	**91.97 ± 1.04**	3.88 ± 1.04	-4.83 ± 1.27

(b) Unsupervised online (epochs = 1) domain incremental learning

Table 2: Summary of (n=10 trials; mean and standard deviation of scores) results for class-incremental and domain incremental variant of vanilla SOM, DendSOM, and contSOM. For DendSOM, we created $n = 4$ soms with unit size = 14

Cifar-10 Model	ACC (↑)	LA (↑)	FM (↓)	BWT (↓)
Finetune	10 ± 0	37.49 ± 0	27.83 ± 0	-30.54 ± 0
Replay	14.84 ± 1.7E-15	87.86 ± 1.42E-14	73.64 ± 0	-81.13 ± 0
LwF	9.87 ± 0.17	11.37 ± 1.04	**1.56 ± 1.31**	**-1.66 ± 1.36**
iCarl	10 ± 0	90.65 ± 1.42E-14	80.65 ± 0	-89.61 ± 1.42E-14
EWC	10.11 ± 0	43.93 ± 7.1E-15	35.69 ± 0	-37.57 ± 0
Memo	11.42 ± 0.48	96.59 ± 2.22	85.17 ± 1.74	-94.64 ± 1.94
Podnet	12.55 ± 1.7E-15	77.47 ± 0	64.92 ± 0	-72.13 ± 0
BiC	12.86 ± 0.72	**96.77 ± 0.99**	83.91 ± 1	-93.24 ± 1.11
SCALE	29.54 ± 0.6	47.31 ± 3.21	20.23 ± 2.11	-19.75 ± 3.52
CSOM	**31.3** ± 0.3	46.14 ± 0.48	14.92 ± 0.24	-16.49 ± 0.25

Table 3: Summary (trials=10) of online (epochs=1) class incremental training on split-Cifar10

memories acquired by our SOM model(s) in Figure 3, which qualitatively demonstrates the types of memories these specific models acquire during learning – for datasets such as Split-MNIST, the SOM only has stored in its internal memories prototypes/templates that match the last few digits/tasks of the underlying task sequence, i.e., largely the digit "8" and "9".

Papers	convolution	buffer storage	Data Augmentation	single pass	class labels	task boundaries
Finetune	✓	✗	✗	✗	✓	✗
Replay	✓	✓	✗	✗	✓	✓
LwF Li & Hoiem (2018)	✓	✗	✗	✗	✓	✓
iCarl Rebuffi et al. (2017)	✓	✓	✗	✗	✓	✓
EWC Kirkpatrick et al. (2017)	✗	✗	✗	✗	✓	✓
Memo Zhou et al. (2023b)	✓	✓	✗	✗	✓	✓
Podnet Douillard et al. (2020)	{✓, ✗}	✓	✗	✗	✓	✓
BiC Wu et al. (2019)	✓	✓	✗	✗	✓	✓
SCALE Yu et al. (2022)	✓	✓	✓	✓	✗	✗
CSOM	✗	✗	✗	✓	✗	✗

Table 4: Training schemes followed by all approaches

The CSOM: The conventional distance metrics, such as euclidean distance or cosine similarity, often identify one of the previously trained units as the BMU for the current incoming task samples due to the semantic overlap present among different task samples in datasets like MNIST (as explained in section 5.1). This means that the images from different classes in MNIST-like datasets appear to be quite similar due to the common black background and white foreground. This increases the probability of an already trained SOM unit to be selected as BMU for an input sample from new class instead of an untrained unit being selected as BMU. Thus, a vanilla SOM fails to use its full capacity and ultimately does not train on all the available units in a continual learning setting. The distance function shown in the Train() subroutine of algorithm 2, divides the squared terms of the L2 distance by the running standard deviation of units obtained from $\mathbf{M}^{\sigma}$. This helps to preserve the trained units' memories (with respect to previously encountered classes) and successfully allocates the untrained units in the SOM to new incoming tasks. In other words, such a distance metric for identifying BMU helps to balance the stability and plasticity of the neural system. More importantly, it eliminates the need for a task vector (refer to Table 4), which sets up context for the incoming tasks in most modern-day continual learning models. As a result, the CSOM can learn in a streaming manner without needing task boundaries which makes it a powerful, unsupervised lifelong learning system.

Experimentally, we noticed that the Gaussian function used to scale the synaptic weight updates in a neighbourhood was liable to cause leaky weight updates in the units that were very far away from the BMU in topology. This caused an explosion of weight update in the available untrained units, thus undesirably increasing the size of cluster for current incoming task. To control this behaviour, we enforced a hard bound over the synaptic weight update in the neighbourhood using the current σ_u value of the BMU. For this we create a binary mask as shown in step 6 of Update() subroutine in Algorithm 2.

In Table 3, we present a comparison of model performance measurements on the split-CIFAR10 benchmark. We used PyCIL Zhou et al. (2023a) to obtain all the benchmarks for standard continual learning models except SCALE Yu et al. (2022). For them, we kept the same setting of total memory size=2000 and memory per class=20. These were the standard parameter settings that Zhou et al. (2023a) used to obtain their baseline results. We conducted 10 experimental trials for all the benchmarks and, after every trial, we constructed a task matrix in order to calculate the ACC, LA, FM, and BWT values for any model. Among all the benchmarks, Yu et al. (2022) had the exact same setting (shown in Table 4) as ours and had state-of-the-art (SOTA) ACC values in a semi-supervised learning setting. Although it had marginally higher mean LA value, their standard deviation was almost 7 times higher than our CSOM after 10 trials. Except for EWC Kirkpatrick et al. (2017), all of the models used convolution and most of them used a storage buffer (memory). Nevertheless, our CSOM model yielded the best average accuracy among all others without maintaining any buffer storage or requiring convolution to obtain better performance, despite operating in an online setting (epochs=1, each input sample processed once).

As shown in Figure 3, as a result of the neural clusters formed, our model appeared to acquire a good latent representation of every input task. This means that there is a good amount of variance among the trained units allocated for every task. However, despite our good experimental results, we could not obtain an equal

number of trained units per class. Moreover, some neuronal units (especially those at the line of separability of clusters) have fuzzy representations. This may occur if a neuronal unit receives a weight update that corresponds to multiple different classes.

Nevertheless, as indicated in Table 2 and 3, **the CSOM achieves the best performance compared to all of the other models/variants of SOM on all four benchmarks/datasets and successfully beats the SOTA model on split-CIFAR10 dataset**. This empirical result indicates that our CSOM framework, leveraging a competitive learning scheme, can yield the potentially best memory retention (or greatest reduction in forgetting) when processing classes incrementally from a data stream. The visualization of the samples synthesized for this particular model – see Figure 3 – also corroborate this result qualitatively; the samples, in this case, look the clearest and the model's internal units seem to represent most of the individual classes/tasks (including those presented at the start of the task sequence).

Discussion: The nature of the distance function and the hyperparameter decay method used in all the SOM models induces an inherent bias towards the initially encountered classes in the class incremental setting. Specifically, it assigns a larger cluster or more trained units in the SOM to initial classes compared to classes that appear later in the incremental order. Although the proposed CSOM produced the best results out of all of the model variants, further improvement is certainly possible in order to obtain clearer/crisper representations of input samples in a trained model final output of a trained SOM (this will be the subject of future work). By augmenting the SOM's internal dynamics with additional synaptic parameters that maintained the running variance for all of its neuronal units, we show that the CSOM can further be used as a useful generative model, facilitating a natural internal memory replay mechanism that could further aid in memory retention in more complex continual learning setups. Notably, this could be an important component to improve the performance of memory-augmented neural networks Das et al. (1992); Graves et al. (2014); Joulin & Mikolov (2015); Mali et al. (2020); Stogin et al. (2024).

6 Conclusions

In this paper, we investigated catastrophic forgetting – a phenomenon where a neural-based intelligent agent forgets the information/knowledge that it acquired on previous datasets/tasks whenever it starts processing a new dataset/task – in the context of continual unsupervised learning utilizing the classical self-organizing map (SOM). Specifically, we designed an adaptation of the classical model to this setting and empirically found that it exhibited severe interference and low memory retention. In light of this, we proposed a novel generalization of the model – the continual SOM (CSOM) – which we theoretically and experimentally demonstrated, across several data benchmarks, that it exhibited vastly improved memory retention ability notably through the use of running variance and decay mechanisms, locally embedded into each neuronal unit. Future work will include an examination of the integration of the cross-task memory retention ability of our model into supervised and semi-supervised neural systems on additional, larger-scale data problems, as well as further improving the quality of the CSOM's internally acquired neural prototypes through additional extensions/generalizations of its local unit-variance parameters.

References

Sumeet Agarwal, Vijaya V. Saradhi, and Harish Karnick. Kernel-based online machine learning and support vector reduction. In *The European Symposium on Artificial Neural Networks*, 2008. URL https://api.semanticscholar.org/CorpusID:3910993.

Rahaf Aljundi, Klaas Kelchtermans, and Tinne Tuytelaars. Task-free continual learning. *2019 IEEE/CVF Conference on Computer Vision and Pattern Recognition (CVPR)*, pp. 11246–11255, 2018. URL https://api.semanticscholar.org/CorpusID:54462131.

Ali Ayub and Alan Wagner. {EEC}: Learning to encode and regenerate images for continual learning. In *International Conference on Learning Representations*, 2021. URL https://openreview.net/forum?id=lWaz5a9lcFU.

Fernando Bação, Victor Lobo, and Marco Painho. Self-organizing maps as substitutes for k-means clustering. In *Computational Science–ICCS 2005: 5th International Conference, Atlanta, GA, USA, May 22-25, 2005, Proceedings, Part III 5*, pp. 476–483. Springer, 2005.

Pouya Bashivan, Martin Schrimpf, Robert Ajemian, Irina Rish, Matthew Riemer, and Yuhai Tu. Continual learning with self-organizing maps. *arXiv preprint arXiv:1904.09330*, 2019.

Ege Beyazit, Jeevithan Alagurajah, and Xindong Wu. Online learning from data streams with varying feature spaces. In *Proceedings of the Thirty-Third AAAI Conference on Artificial Intelligence and Thirty-First Innovative Applications of Artificial Intelligence Conference and Ninth AAAI Symposium on Educational Advances in Artificial Intelligence*, AAAI'19/IAAI'19/EAAI'19. AAAI Press, 2019. ISBN 978-1-57735-809-1. doi: 10.1609/aaai.v33i01.33013232. URL https://doi.org/10.1609/aaai.v33i01.33013232.

Amirreza Bigdeli, Abbas Maghsoudi, and Reza Ghezelbash. Application of self-organizing map (som) and k-means clustering algorithms for portraying geochemical anomaly patterns in moalleman district, ne iran. *Journal of Geochemical Exploration*, 233:106923, 2022.

Matteo Boschini, Lorenzo Bonicelli, Pietro Buzzega, Angelo Porrello, and Simone Calderara. Class-incremental continual learning into the extended der-verse. *IEEE Transactions on Pattern Analysis and Machine Intelligence*, 45(5):5497–5512, 2023. doi: 10.1109/TPAMI.2022.3206549.

TA Burton. Stability by fixed point theory or liapunov's theory: A comparison. *Fixed point theory*, 4(1): 15–32, 2003.

Zhiyuan Chen and Bing Liu. Lifelong machine learning. *Synthesis Lectures on Artificial Intelligence and Machine Learning*, 10(3):1–145, 2016.

Yoonsuck Choe. *Hebbian Learning*, pp. 1–5. Springer New York, New York, NY, 2013. ISBN 978-1-4614-7320-6. doi: 10.1007/978-1-4614-7320-6_672-1. URL https://doi.org/10.1007/978-1-4614-7320-6_672-1.

Tarin Clanuwat, Mikel Bober-Irizar, Asanobu Kitamoto, Alex Lamb, Kazuaki Yamamoto, and David Ha. Deep learning for classical japanese literature. *ArXiv*, abs/1812.01718, 2018. URL https://api.semanticscholar.org/CorpusID:54458639.

Sreerupa Das, C Giles, and Guo-Zheng Sun. Using prior knowledge in a nnpda to learn context-free languages. *Advances in neural information processing systems*, 5, 1992.

Arthur Douillard, Matthieu Cord, Charles Ollion, Thomas Robert, and Eduardo Valle. Podnet: Pooled outputs distillation for small-tasks incremental learning. In *Computer Vision – ECCV 2020: 16th European Conference, Glasgow, UK, August 23–28, 2020, Proceedings, Part XX*, pp. 86–102, Berlin, Heidelberg, 2020. Springer-Verlag. ISBN 978-3-030-58564-8. doi: 10.1007/978-3-030-58565-5_6. URL https://doi.org/10.1007/978-3-030-58565-5_6.

Edward W Forgy. Cluster analysis of multivariate data: efficiency versus interpretability of classifications. *biometrics*, 21:768–769, 1965.

Robert M French. Catastrophic forgetting in connectionist networks. *Trends in cognitive sciences*, 3(4): 128–135, 1999.

Bernd Fritzke. A growing neural gas network learns topologies. In *Proceedings of the 7th International Conference on Neural Information Processing Systems*, NIPS'94, pp. 625–632, Cambridge, MA, USA, 1994. MIT Press.

Alexander Gepperth, Thomas Hecht, Mathieu Lefort, and Ursula Korner. Biologically inspired incremental learning for high-dimensional spaces. In *2015 Joint IEEE International Conference on Development and Learning and Epigenetic Robotics (ICDL-EpiRob)*, pp. 269–275, 2015. doi: 10.1109/DEVLRN.2015.7346155.

Valentina Gliozzi and Kim Plunkett. Self-organizing maps and generalization: an algorithmic description of numerosity and variability effects. *arXiv preprint arXiv:1802.09442*, 2018.

Alex Graves, Greg Wayne, and Ivo Danihelka. Neural turing machines. *arXiv preprint arXiv:1410.5401*, 2014.

Robert Gray. Vector quantization. *IEEE Assp Magazine*, 1(2):4–29, 1984.

Rudolf Haag, Daniel Kastler, and Ewa B Trych-Pohlmeyer. Stability and equilibrium states. *Communications in Mathematical Physics*, 38:173–193, 1974.

Pitoyo Hartono. *Competitive Learning*, pp. 671–677. Springer US, Boston, MA, 2012. ISBN 978-1-4419-1428-6. doi: 10.1007/978-1-4419-1428-6_175. URL https://doi.org/10.1007/978-1-4419-1428-6_175.

Tyler L. Hayes, Nathan D. Cahill, and Christopher Kanan. Memory efficient experience replay for streaming learning. In *2019 International Conference on Robotics and Automation (ICRA)*, pp. 9769–9776, 2019. doi: 10.1109/ICRA.2019.8793982.

Donald O Hebb et al. The organization of behavior, 1949.

David Isele and Akansel Cosgun. Selective experience replay for lifelong learning. In *AAAI*, 2018.

Armand Joulin and Tomas Mikolov. Inferring algorithmic patterns with stack-augmented recurrent nets. *Advances in neural information processing systems*, 28, 2015.

Lyes Khacef, Laurent Rodriguez, and Benoît Miramond. Improving self-organizing maps with unsupervised feature extraction. In *International Conference on Neural Information Processing*, pp. 474–486. Springer, 2020.

James Kirkpatrick, Razvan Pascanu, Neil Rabinowitz, Joel Veness, Guillaume Desjardins, Andrei A Rusu, Kieran Milan, John Quan, Tiago Ramalho, Agnieszka Grabska-Barwinska, et al. Overcoming catastrophic forgetting in neural networks. *Proceedings of the national academy of sciences*, 114(13):3521–3526, 2017.

Teuvo Kohonen. Self-organized formation of topologically correct feature maps. *Biological cybernetics*, 43(1): 59–69, 1982.

Dorota Celińska-Kopczyńska Eryk Kopczyński. Non-euclidean self-organizing maps. *arXiv preprint arXiv:2109.11769*, 2021.

Alex Krizhevsky and Geoff Hinton. Convolutional deep belief networks on cifar-10. *Unpublished manuscript*, 40(7):1–9, 2010.

Yann LeCun, Léon Bottou, Yoshua Bengio, and Patrick Haffner. Gradient-based learning applied to document recognition. *Proc. IEEE*, 86:2278–2324, 1998. URL https://api.semanticscholar.org/CorpusID:14542261.

Xiaorong Li, Shipeng Wang, Jian Sun, and Zongben Xu. Variational data-free knowledge distillation for continual learning. *IEEE Transactions on Pattern Analysis and Machine Intelligence*, 45(10):12618–12634, 2023. doi: 10.1109/TPAMI.2023.3271626.

Zhizhong Li and Derek Hoiem. Learning without forgetting. *IEEE Transactions on Pattern Analysis and Machine Intelligence*, 40(12):2935–2947, 2018. doi: 10.1109/TPAMI.2017.2773081.

Shaoshan Liu, Liangkai Liu, Jie Tang, Bo Yu, Yifan Wang, and Weisong Shi. Edge computing for autonomous driving: Opportunities and challenges. *Proceedings of the IEEE*, 107(8):1697–1716, 2019.

Stuart Lloyd. Least squares quantization in pcm. *IEEE transactions on information theory*, 28(2):129–137, 1982.

David Lopez-Paz and Marc'Aurelio Ranzato. Gradient episodic memory for continual learning. In *Proceedings of the 31st International Conference on Neural Information Processing Systems*, NIPS'17, pp. 6470–6479, Red Hook, NY, USA, 2017a. Curran Associates Inc. ISBN 9781510860964.

David Lopez-Paz and Marc'Aurelio Ranzato. Gradient episodic memory for continual learning. *Advances in neural information processing systems*, 30:6467–6476, 2017b.

Zimeng Lyu, Alexander Ororbia, Rui Li, and Travis Desell. Minimally supervised learning using topological projections in self-organizing maps. *arXiv preprint arXiv:2401.06923*, 2024.

Ankur Arjun Mali, Alexander G Ororbia II, and C Lee Giles. A neural state pushdown automata. *IEEE Transactions on Artificial Intelligence*, 1(3):193–205, 2020.

Thomas Martinetz. Competitive hebbian learning rule forms perfectly topology preserving maps. In *International conference on artificial neural networks*, pp. 427–434. Springer, 1993.

Marc Masana, Xialei Liu, Bartłomiej Twardowski, Mikel Menta, Andrew D. Bagdanov, and Joost van de Weijer. Class-incremental learning: Survey and performance evaluation on image classification. *IEEE Transactions on Pattern Analysis and Machine Intelligence*, 45(5):5513–5533, 2023. doi: 10.1109/TPAMI.2022.3213473.

Michael McCloskey and Neal J. Cohen. Catastrophic interference in connectionist networks: The sequential learning problem. *The psychology of learning and motivation*, 24(109):92, 1989.

Martial Mermillod, Aurélia Bugaiska, and Patrick Bonin. The stability-plasticity dilemma: investigating the continuum from catastrophic forgetting to age-limited learning effects. *Frontiers in Psychology*, 4:504, 2013. ISSN 1664-1078. doi: 10.3389/fpsyg.2013.00504. URL `https://www.frontiersin.org/article/10.3389/fpsyg.2013.00504`.

Alex Ororbia, Ankur Mali, C Lee Giles, and Daniel Kifer. Lifelong neural predictive coding: Learning cumulatively online without forgetting. *Advances in Neural Information Processing Systems*, 35:5867–5881, 2022.

Alexander Ororbia, Ankur Mali, C Lee Giles, and Daniel Kifer. Continual learning of recurrent neural networks by locally aligning distributed representations. *IEEE transactions on neural networks and learning systems*, 31(10):4267–4278, 2020.

Alexander G Ororbia. Continual competitive memory: A neural system for online task-free lifelong learning. *arXiv preprint arXiv:2106.13300*, 2021.

Alexander G Ororbia. Brain-inspired machine intelligence: A survey of neurobiologically-plausible credit assignment. *arXiv preprint arXiv:2312.09257*, 2023.

Quang Pham, Chenghao Liu, and Steven C. H. Hoi. Continual learning, fast and slow. *IEEE Transactions on Pattern Analysis and Machine Intelligence*, 46(1):134–149, 2024. doi: 10.1109/TPAMI.2023.3324203.

Kosmas Pinitas, Spyridon Chavlis, and Panayiota Poirazi. Dendritic self-organizing maps for continual learning. *arXiv preprint arXiv:2110.13611*, 2021a.

Kosmas Pinitas, Spyridon Chavlis, and Panayiota Poirazi. Dendritic self-organizing maps for continual learning. *arXiv preprint arXiv:2110.13611*, 2021b.

Roger Ratcliff. Connectionist models of recognition memory: constraints imposed by learning and forgetting functions. *Psychological review*, 97(2):285, 1990.

Sylvestre-Alvise Rebuffi, Alexander Kolesnikov, Georg Sperl, and Christoph H. Lampert. icarl: Incremental classifier and representation learning. In *2017 IEEE Conference on Computer Vision and Pattern Recognition (CVPR)*, pp. 5533–5542, 2017. doi: 10.1109/CVPR.2017.587.

Nicolas P Rougier and Georgios Is Detorakis. Randomized self-organizing map. *Neural Computation*, 33(8): 2241–2273, 2021.

David E Rumelhart, James L McClelland, and CORPORATE PDP Research Group. *Parallel distributed processing: Explorations in the microstructure of cognition, Vol. 1: Foundations*. MIT press, 1986.

Hanul Shin, Jung Kwon Lee, Jaehong Kim, and Jiwon Kim. Continual learning with deep generative replay. In *Proceedings of the 31st International Conference on Neural Information Processing Systems*, NIPS'17, pp. 2994–3003, Red Hook, NY, USA, 2017. Curran Associates Inc. ISBN 9781510860964.

Rupesh K Srivastava, Jonathan Masci, Sohrob Kazerounian, Faustino Gomez, and Jürgen Schmidhuber. Compete to compute. *Advances in neural information processing systems*, 26, 2013.

John Stogin, Ankur Mali, and C Lee Giles. A provably stable neural network turing machine with finite precision and time. *Information Sciences*, 658:120034, 2024.

Sebastian Thrun and Tom M Mitchell. Lifelong robot learning. *Robotics and autonomous systems*, 15(1-2): 25–46, 1995.

Elio Ventocilla, Rafael M. Martins, Fernando Paulovich, and Maria Riveiro. Scaling the growing neural gas for visual cluster analysis. *Big Data Research*, 26:100254, 2021. ISSN 2214-5796. doi: https://doi.org/10.1016/j.bdr.2021.100254. URL https://www.sciencedirect.com/science/article/pii/S221457962100071X.

Juha Vesanto and Esa Alhoniemi. Clustering of the self-organizing map. *IEEE Transactions on neural networks*, 11(3):586–600, 2000.

Zhenyi Wang, Li Shen, Tiehang Duan, Qiuling Suo, Le Fang, Wei Liu, and Mingchen Gao. Distributionally robust memory evolution with generalized divergence for continual learning. *IEEE Transactions on Pattern Analysis and Machine Intelligence*, 45(12):14337–14352, 2023. doi: 10.1109/TPAMI.2023.3317874.

BP Welford. Note on a method for calculating corrected sums of squares and products. *Technometrics*, 4(3): 419–420, 1962.

Yue Wu, Yinpeng Chen, Lijuan Wang, Yuancheng Ye, Zicheng Liu, Yandong Guo, and Yun Fu. Large scale incremental learning. In *Proceedings of the IEEE/CVF Conference on Computer Vision and Pattern Recognition (CVPR)*, June 2019.

Han Xiao, Kashif Rasul, and Roland Vollgraf. Fashion-mnist: a novel image dataset for benchmarking machine learning algorithms. *ArXiv*, abs/1708.07747, 2017. URL https://api.semanticscholar.org/CorpusID:702279.

Ju Xu, Jin Ma, Xuesong Gao, and Zhanxing Zhu. Adaptive progressive continual learning. *IEEE Transactions on Pattern Analysis and Machine Intelligence*, 44(10):6715–6728, 2022. doi: 10.1109/TPAMI.2021.3095064.

Boyu Yang, Mingbao Lin, Yunxiao Zhang, Binghao Liu, Xiaodan Liang, Rongrong Ji, and Qixiang Ye. Dynamic support network for few-shot class incremental learning. *IEEE Transactions on Pattern Analysis and Machine Intelligence*, 45(3):2945–2951, 2023. doi: 10.1109/TPAMI.2022.3175849.

Fei Ye and Adrian G. Bors. Dynamic self-supervised teacher-student network learning. *IEEE Transactions on Pattern Analysis and Machine Intelligence*, 45(5):5731–5748, 2023. doi: 10.1109/TPAMI.2022.3220928.

Haiyan Yin, Peng Yang, and Ping Li 0001. Mitigating forgetting in online continual learning with neuron calibration. In Marc'Aurelio Ranzato, Alina Beygelzimer, Yann N. Dauphin, Percy Liang, and Jennifer Wortman Vaughan (eds.), *Advances in Neural Information Processing Systems 34: Annual Conference on Neural Information Processing Systems 2021, NeurIPS 2021, December 6-14, 2021, virtual*, pp. 10260–10272, 2021. URL https://proceedings.neurips.cc/paper/2021/hash/54ee290e80589a2a1225c338a71839f5-Abstract.html.

Xiaofan Yu, Yunhui Guo, Sicun Gao, and Tajana Simunic. Scale: Online self-supervised lifelong learning without prior knowledge. *2023 IEEE/CVF Conference on Computer Vision and Pattern Recognition Workshops (CVPRW)*, pp. 2484–2495, 2022. URL https://api.semanticscholar.org/CorpusID:251765472.

Da-Wei Zhou, Fu-Yun Wang, Han-Jia Ye, and De-Chuan Zhan. Pycil: a python toolbox for class-incremental learning. *SCIENCE CHINA Information Sciences*, 66(9):197101–, 2023a. doi: https://doi.org/10.1007/s11432-022-3600-y.

Da-Wei Zhou, Qi-Wei Wang, Han-Jia Ye, and De-Chuan Zhan. A model or 603 exemplars: Towards memory-efficient class-incremental learning. In *The Eleventh International Conference on Learning Representations*, 2023b. URL https://openreview.net/forum?id=S07feAlQHgM.

A Appendix

Revisiting the hyperparameters defined:
Table 5 indicates key notations, symbols and abbreviations used in this paper.

Item	Explanation
$\mathcal{G} = (K \times L)$	Network Topology (dimensions of the SOM)
	NOTE: $K = L$ for CSOM
D	unit/neuron size and size of individual input sample
$\mathbf{M} \in \mathcal{R}^{D \times H}$	synaptic matrix of SOM
u	Best Matching Unit (BMU)
v_j	a non-BMU at location j in CSOM
$V = \{v_j \mid 0 < j < K^2\}$	all non-BMU units in CSOM
$H = \{u\} \cup V$	all units in the SOM
σ_0	initial radius for all neurons
λ_0	initial learning rate all neurons
σ_u and σ_v	radius of BMU and radius of non-BMU neuron
λ_u and λ_v	learning rate of BMU and learning rate of non-BMU neuron
ω^2	running variance of a neuron
$\mathbf{M}^{\omega^2} \in \mathcal{R}^{D \times H}$	matrix of running variance of all neurons in SOM
$\sigma_h = \{\sigma_u\} \cup \{\sigma_{v_j}\} \in \mathcal{R}^{1 \times H}$	radius of all neurons for weight update
$\lambda_h = \{\lambda_u\} \cup \{\lambda_{v_j}\} \in \mathcal{R}^{1 \times H}$	learning rate for all neurons used in the weight update steps of CSOM
λ_ω^0	initial scaling/update factor for updating the running variance of every unit
λ_ω	adjusted scaling/update factor for updating the running variance of every unit
τ_σ	time constant for radius
τ_λ	time constant for learning rate
p	patch size (DendSOM)
s	stride length (DendSOM)

Table 5: Notations, Symbols, abbreviations used in this paper

Note that the DendSOM benchmarks are our implementation of the model, as the original source code was not publicly available.

A.1 Class Incremental Learning

This section contains information about class incremental settings where each task size had exactly one class in it.

A.1.1 MNIST

Hyperparameters: Table 6 contains the empirically obtained initial hyperparameters for obtaining the best possible results as described in Table 2a.

Model	H	D	σ_0	λ_0	ω_0^2	λ_ω^0	τ_σ	τ_λ	p	s
Vanilla SOM	15×15	28×28	0.6	0.07	1	0.9	8	45	-	-
DendSOM	8×8	$7 \times [14 \times 14]$	4	0.95	2	0.005	-	-	10	3
CSOM	15×15	28×28	1.5	0.07	0.5	0.9	8	45	-	-

Table 6: Hyperparameters for Class Incremental setting on MNIST

Task matrices: We performed 10 trials of CSOM trained on MNIST. Table 7 indicates the resultant accuracy values,

100.0 ± 0.0	0.0 ± 0.0	0.0 ± 0.0	0.0 ± 0.0	0.0 ± 0.0	0.0 ± 0.0	0.0 ± 0.0	0.0 ± 0.0	0.0 ± 0.0	0.0 ± 0.0
99.77 ± 0.12	99.89 ± 0.14	0.0 ± 0.0	0.0 ± 0.0	0.0 ± 0.0	0.0 ± 0.0	0.0 ± 0.0	0.0 ± 0.0	0.0 ± 0.0	0.0 ± 0.0
99.17 ± 0.4	99.41 ± 0.31	96.91 ± 1.2	0.0 ± 0.0	0.0 ± 0.0	0.0 ± 0.0	0.0 ± 0.0	0.0 ± 0.0	0.0 ± 0.0	0.0 ± 0.0
98.83 ± 0.54	99.23 ± 0.31	93.31 ± 2.98	96.01 ± 1.41	0.0 ± 0.0	0.0 ± 0.0	0.0 ± 0.0	0.0 ± 0.0	0.0 ± 0.0	0.0 ± 0.0
98.78 ± 0.52	99.22 ± 0.32	92.26 ± 3.38	94.61 ± 1.8	96.34 ± 1.02	0.0 ± 0.0	0.0 ± 0.0	0.0 ± 0.0	0.0 ± 0.0	0.0 ± 0.0
96.78 ± 3.13	99.07 ± 0.43	92.12 ± 3.39	84.99 ± 9.97	96.05 ± 1.02	88.98 ± 5.21	0.0 ± 0.0	0.0 ± 0.0	0.0 ± 0.0	0.0 ± 0.0
95.96 ± 3.0	98.5 ± 1.22	89.5 ± 6.05	84.52 ± 10.0	95.39 ± 1.19	86.19 ± 6.37	94.8 ± 2.46	0.0 ± 0.0	0.0 ± 0.0	0.0 ± 0.0
95.93 ± 2.99	98.5 ± 1.22	88.33 ± 6.72	83.39 ± 10.11	93.3 ± 2.96	85.32 ± 6.34	94.75 ± 2.48	92.54 ± 1.59	0.0 ± 0.0	0.0 ± 0.0
95.93 ± 3.03	98.41 ± 1.19	87.09 ± 6.55	81.73 ± 9.47	93.05 ± 3.07	80.09 ± 9.43	93.6 ± 4.35	92.42 ± 1.6	84.72 ± 2.25	0.0 ± 0.0
95.89 ± 3.02	98.41 ± 1.19	87.14 ± 6.55	81.39 ± 9.33	79.17 ± 8.47	79.53 ± 9.35	93.36 ± 4.28	80.64 ± 7.77	82.43 ± 3.17	72.37 ± 14.48

Table 7: mean and standard deviation of accuracies in a task matrix

A.1.2 KMNIST

Hyperparameters: Table 8 shows the hyperparameters we used for obtaining the results in Table 2a on KMNIST dataset.

Model	H	D	σ_0	λ_0	ω_0^2	λ_ω^0	τ_σ	τ_λ	p	s
Vanilla SOM	20×20	28×28	0.6	0.07	1	0.9	8	45	-	-
DendSOM	10×10	$7 \times [14 \times 14]$	6	0.95	2	0.005	-	-	4	2
CSOM	35×35	28×28	1.5	0.07	0.5	0.9	8	45	-	-

Table 8: Hyperparameters for Class Incremental setting on KMNIST

Task matrices: We performed 10 trials of CSOM trained on KMNIST. Table 9 indicates the resultant accuracy values,

100.0 ± 0.0	0.0 ± 0.0	0.0 ± 0.0	0.0 ± 0.0	0.0 ± 0.0	0.0 ± 0.0	0.0 ± 0.0	0.0 ± 0.0	0.0 ± 0.0	0.0 ± 0.0
98.08 ± 0.85	98.72 ± 0.71	0.0 ± 0.0	0.0 ± 0.0	0.0 ± 0.0	0.0 ± 0.0	0.0 ± 0.0	0.0 ± 0.0	0.0 ± 0.0	0.0 ± 0.0
97.86 ± 0.71	88.0 ± 2.71	93.25 ± 1.14	0.0 ± 0.0	0.0 ± 0.0	0.0 ± 0.0	0.0 ± 0.0	0.0 ± 0.0	0.0 ± 0.0	0.0 ± 0.0
97.44 ± 0.82	88.06 ± 2.81	87.59 ± 1.93	94.2 ± 1.67	0.0 ± 0.0	0.0 ± 0.0	0.0 ± 0.0	0.0 ± 0.0	0.0 ± 0.0	0.0 ± 0.0
93.98 ± 1.22	86.21 ± 3.18	86.63 ± 1.83	93.53 ± 1.66	82.79 ± 1.95	0.0 ± 0.0	0.0 ± 0.0	0.0 ± 0.0	0.0 ± 0.0	0.0 ± 0.0
89.3 ± 3.37	85.93 ± 3.2	84.0 ± 3.27	91.73 ± 2.03	81.15 ± 3.03	82.6 ± 3.57	0.0 ± 0.0	0.0 ± 0.0	0.0 ± 0.0	0.0 ± 0.0
88.97 ± 3.34	83.55 ± 3.24	79.92 ± 3.71	91.27 ± 2.14	79.93 ± 3.2	80.48 ± 3.16	85.91 ± 3.51	0.0 ± 0.0	0.0 ± 0.0	0.0 ± 0.0
86.32 ± 3.14	83.37 ± 3.24	79.42 ± 3.74	91.16 ± 2.19	79.43 ± 3.17	80.33 ± 3.13	85.68 ± 3.49	89.19 ± 1.55	0.0 ± 0.0	0.0 ± 0.0
83.86 ± 3.45	81.31 ± 3.21	77.98 ± 3.72	90.45 ± 2.68	77.59 ± 3.58	79.34 ± 3.38	83.33 ± 4.9	87.31 ± 2.63	80.75 ± 4.35	0.0 ± 0.0
83.75 ± 3.41	80.35 ± 3.18	77.21 ± 3.98	90.39 ± 2.72	75.72 ± 4.39	79.28 ± 3.41	83.25 ± 4.92	86.62 ± 2.2	80.79 ± 4.36	78.66 ± 4.79

Table 9: mean and standard deviation of accuracies in a task matrix

A.1.3 Fashion-MNIST

Hyperparameters: Table 10 indicates the hyperparameters used for obtaining results in Table 2a on Fashion-MNIST dataset.

A.1.4 CIFAR10

Hyperparameters: Table 12 indicates the hyperparameters used to obtain results in Table 3 the on split-CIFAR10 dataset.

Table 13 indicates hyperparameters set while implementing models from Zhou et al. (2023a) in a Class Incremental Online Learning setting.

Apart from the hyperparameters mentioned in Tables 13 and 14, the rest of the hyperparameters were unchanged in their publicly available code. We added an evaluation code for obtaining task matrices for all the models in Table 3.

Task matrices: We performed 8 trials of CSOM trained on CIFAR-10. Following resultant accuracies values.

Model	H	D	σ_0	λ_0	ω_0^2	λ_ω^0	τ_σ	τ_λ	p	s
Vanilla SOM	20×20	28×28	0.6	0.07	1	0.9	8	45	-	-
DendSOM	10×10	$7 \times [14 \times 14]$	5	0.95	2	0.005	-	-	8	4
CSOM	25×25	28×28	1.5	0.07	0.5	0.9	8	45	-	-

Table 10: Hyperparameters for Class Incremental setting on Fashion-MNIST

100.0 ± 0.0	0.0 ± 0.0	0.0 ± 0.0	0.0 ± 0.0	0.0 ± 0.0	0.0 ± 0.0	0.0 ± 0.0	0.0 ± 0.0	0.0 ± 0.0	0.0 ± 0.0
97.39 ± 1.49	97.7 ± 0.59	0.0 ± 0.0	0.0 ± 0.0	0.0 ± 0.0	0.0 ± 0.0	0.0 ± 0.0	0.0 ± 0.0	0.0 ± 0.0	0.0 ± 0.0
92.9 ± 1.91	96.72 ± 0.82	94.32 ± 0.71	0.0 ± 0.0	0.0 ± 0.0	0.0 ± 0.0	0.0 ± 0.0	0.0 ± 0.0	0.0 ± 0.0	0.0 ± 0.0
85.83 ± 3.25	88.44 ± 6.73	93.67 ± 0.72	89.49 ± 3.6	0.0 ± 0.0	0.0 ± 0.0	0.0 ± 0.0	0.0 ± 0.0	0.0 ± 0.0	0.0 ± 0.0
85.71 ± 2.99	88.34 ± 6.68	73.42 ± 4.09	83.11 ± 4.61	76.2 ± 3.7	0.0 ± 0.0	0.0 ± 0.0	0.0 ± 0.0	0.0 ± 0.0	0.0 ± 0.0
85.64 ± 3.03	88.34 ± 6.68	73.49 ± 4.08	83.07 ± 4.58	75.93 ± 3.79	99.76 ± 0.11	0.0 ± 0.0	0.0 ± 0.0	0.0 ± 0.0	0.0 ± 0.0
77.5 ± 3.31	88.34 ± 6.69	68.65 ± 3.46	82.88 ± 4.54	72.45 ± 3.56	99.6 ± 0.39	41.62 ± 2.74	0.0 ± 0.0	0.0 ± 0.0	0.0 ± 0.0
77.51 ± 3.32	88.34 ± 6.69	68.65 ± 3.48	82.88 ± 4.54	72.45 ± 3.56	66.87 ± 13.25	41.55 ± 2.73	95.77 ± 3.74	0.0 ± 0.0	0.0 ± 0.0
77.24 ± 3.24	88.33 ± 6.68	68.57 ± 3.48	82.62 ± 4.61	72.11 ± 3.42	66.83 ± 13.1	39.95 ± 2.75	90.12 ± 9.74	94.84 ± 0.94	0.0 ± 0.0
77.23 ± 3.21	88.34 ± 6.66	68.53 ± 3.47	82.6 ± 4.59	72.08 ± 3.4	58.84 ± 14.3	39.87 ± 2.69	76.89 ± 11.12	94.28 ± 1.19	92.65 ± 2.89

Table 11: mean and standard deviation of accuracies in a task matrix

Model	H	D	σ_0	λ_0	ω_0^2	λ_ω^0	τ_σ	τ_λ
CSOM	100×100	32×32	1.5	0.2	0.6	0.9	6	45

Table 12: Hyperparameters for CSOM for Class Incremental setting on CIFAR10

Papers	Memory Size	Memory per Class	Model	epochs	Fixed Memory
Finetune, Replay, LwF, iCarl, EWC, Memo, Podnet, BiC	2000	20	Resnet32	1	✗

Table 13: Hyperparameters for benchmarks from PyCIL Zhou et al. (2023a) on CIFAR10

Paper	Model	Data setting	lr	epochs	memory size
SCALE	Resnet18	*seq*	0.03	1	256

Table 14: Hyperparameters for benchmarks from SCALE Yu et al. (2022) using SGD optimizer

100.0 ± 0.0	0.0 ± 0.0	0.0 ± 0.0	0.0 ± 0.0	0.0 ± 0.0	0.0 ± 0.0	0.0 ± 0.0	0.0 ± 0.0	0.0 ± 0.0	0.0 ± 0.0
84.2 ± 1.55	76.88 ± 1.22	0.0 ± 0.0	0.0 ± 0.0	0.0 ± 0.0	0.0 ± 0.0	0.0 ± 0.0	0.0 ± 0.0	0.0 ± 0.0	0.0 ± 0.0
65.86 ± 1.37	73.09 ± 1.15	52.61 ± 2.5	0.0 ± 0.0	0.0 ± 0.0	0.0 ± 0.0	0.0 ± 0.0	0.0 ± 0.0	0.0 ± 0.0	0.0 ± 0.0
62.0 ± 1.42	67.05 ± 1.07	41.47 ± 2.12	46.31 ± 1.57	0.0 ± 0.0	0.0 ± 0.0	0.0 ± 0.0	0.0 ± 0.0	0.0 ± 0.0	0.0 ± 0.0
55.48 ± 1.41	65.26 ± 1.14	36.68 ± 1.92	43.8 ± 1.55	22.42 ± 1.16	0.0 ± 0.0	0.0 ± 0.0	0.0 ± 0.0	0.0 ± 0.0	0.0 ± 0.0
53.9 ± 1.59	63.2 ± 0.91	32.28 ± 2.28	32.22 ± 1.68	22.2 ± 0.42	31.49 ± 1.44	0.0 ± 0.0	0.0 ± 0.0	0.0 ± 0.0	0.0 ± 0.0
52.76 ± 1.34	61.82 ± 0.7	30.75 ± 2.13	29.7 ± 1.89	21.41 ± 0.83	31.01 ± 1.5	20.24 ± 1.21	0.0 ± 0.0	0.0 ± 0.0	0.0 ± 0.0
50.96 ± 0.77	59.95 ± 1.06	29.02 ± 1.74	28.08 ± 1.74	19.91 ± 0.96	29.31 ± 1.66	19.79 ± 1.17	37.3 ± 1.09	0.0 ± 0.0	0.0 ± 0.0
42.49 ± 1.07	53.13 ± 1.29	27.98 ± 1.74	27.06 ± 1.25	19.11 ± 1.05	28.64 ± 1.48	19.32 ± 1.05	37.14 ± 0.99	38.04 ± 1.61	0.0 ± 0.0
41.2 ± 1.11	42.96 ± 1.1	27.71 ± 1.59	26.19 ± 1.15	18.74 ± 1.12	28.51 ± 1.18	18.88 ± 0.96	36.25 ± 1.04	36.36 ± 1.65	36.01 ± 0.9

Table 15: mean and standard deviation of accuracies in a task matrix

A.2 Domain Incremental Learning

For the domain incremental setting, we set number of tasks = 5, number of classes/task = 2

A.2.1 MNIST

Hyperparameters: Table 16 contains the initial hyperparameters used for obtaining the results shown in Table 2b.

Task matrices: Table 17 indicates the resultant accuracy values obtained after performing 10 trials.

Model	H	D	σ_0	λ_0	ω_h^2	λ_ω^0	τ_σ	τ_λ	p	s
Vanilla SOM	15×15	28×28	0.6	0.07	1	0.9	8	45	-	-
DendSOM	8×8	$7 \times [14 \times 14]$	4	0.95	2	0.005	-	-	10	3
CSOM	15×15	28×28	1.5	0.07	0.5	0.9	8	45	-	-

Table 16: Hyperparameters for Domain Incremental setting on MNIST

99.85 ± 0.04	45.59 ± 5.94	45.63 ± 3.38	68.99 ± 4.3	39.82 ± 5.51
99.04 ± 1.04	93.57 ± 2.13	61.77 ± 3.29	73.77 ± 10.54	45.9 ± 4.1
97.55 ± 1.65	93.25 ± 2.75	93.88 ± 2.96	55.48 ± 7.08	18.41 ± 3.85
98.1 ± 1.65	92.6 ± 2.78	90.52 ± 5.21	96.94 ± 0.97	29.71 ± 4.53
97.99 ± 1.65	91.85 ± 2.77	77.5 ± 9.88	97.2 ± 0.87	80.92 ± 6.1

Table 17: mean and standard deviation of accuracies in a task matrix

A.2.2 KMNIST

Hyperparameters: Table 18 contains the initial hyperparameters used for obtaining the results shown in Table 2b.

Model	H	D	σ_0	λ_0	ω_h^2	λ_ω^0	τ_σ	τ_λ	p	s
Vanilla SOM	20×20	28×28	0.6	0.07	1	0.9	8	45	-	-
DendSOM	12×12	$7 \times [14 \times 14]$	6	0.95	2	0.005	-	-	4	2
CSOM	35×35	28×28	1.5	0.07	0.5	0.9	8	45	-	-

Table 18: Hyperparameters for Domain Incremental setting on KMNIST

Task matrices: Table 19 indicates the resultant accuracy values obtained after performing 10 trials

A.2.3 Fashion-MNIST

Hyperparameters: Table 20 contains the initial hyperparameters used for obtaining the results shown in Table 2b.

Task matrices: Table 21 indicates the resultant accuracy values obtained after performing 10 trials.

A.2.4 CIFAR-10

Hyperparameters: Table 22 shows hyperparameters used for training CSOM on CIFAR10 in a Domain Incremental Setting.

98.6 ± 0.4	29.35 ± 1.24	54.72 ± 2.57	28.63 ± 2.45	47.21 ± 2.47
92.19 ± 2.46	91.48 ± 1.68	41.84 ± 3.3	55.72 ± 3.25	42.46 ± 2.05
89.91 ± 2.75	89.74 ± 1.99	89.85 ± 2.09	52.24 ± 2.62	39.38 ± 1.62
86.8 ± 2.5	89.55 ± 1.94	88.32 ± 2.21	93.01 ± 1.83	45.63 ± 1.43
86.1 ± 2.69	88.89 ± 2.32	86.72 ± 3.45	91.91 ± 2.87	86.92 ± 2.3

Table 19: mean and standard deviation of accuracies in a task matrix

Model	H	D	σ_0	λ_0	ω_h^2	λ_ω^0	τ_σ	τ_λ	p	s
Vanilla SOM	20×20	28×28	0.6	0.07	1	0.9	8	45	-	-
DendSOM	10×10	$7 \times [14 \times 14]$	5	0.95	2	0.005	-	-	8	4
CSOM	25×25	28×28	1.5	0.07	0.5	0.9	8	45	-	-

Table 20: Hyperparameters for Domain Incremental setting on Fashion-MNIST

96.72 ± 1.44	53.15 ± 6.27	28.88 ± 4.84	40.7 ± 2.94	49.77 ± 0.27
92.63 ± 1.79	95.08 ± 0.61	41.42 ± 1.21	44.46 ± 1.51	47.21 ± 2.26
92.94 ± 1.72	92.22 ± 1.61	97.55 ± 0.87	95.75 ± 1.36	83.07 ± 3.94
93.72 ± 1.71	91.37 ± 1.49	97.58 ± 0.92	97.22 ± 0.86	86.17 ± 4.71
93.96 ± 1.73	90.77 ± 2.15	97.1 ± 0.85	97.06 ± 1.22	99.13 ± 0.13

Table 21: mean and standard deviation of accuracies in a task matrix

Model	H	D	σ_0	λ_0	ω_h^2	λ_ω^0	τ_σ	τ_λ
CSOM	15×15	28×28	1.5	0.07	0.5	0.9	8	45

Table 22: Hyperparameters for Domain Incremental setting on CIFAR10

Table 23 shows task matrix of accuracy values obtained after performing 8 trials of CSOM on grayscale images from CIFAR-10.

99.52 ± 0.37	46.01 ± 4.66	43.63 ± 5.55	65.38 ± 5.11	38.67 ± 6.55
98.79 ± 0.59	93.15 ± 1.09	60.14 ± 2.78	74.98 ± 7.41	50.55 ± 2.84
97.15 ± 1.38	91.67 ± 1.84	94.41 ± 1.08	52.1 ± 7.59	18.99 ± 3.8
95.53 ± 7.62	91.35 ± 1.74	89.13 ± 5.01	95.36 ± 0.72	30.34 ± 3.01
97.25 ± 2.91	91.23 ± 0.92	68.91 ± 5.9	95.85 ± 0.77	79.57 ± 5.46

Table 23: mean and standard deviation of accuracies in a task matrix